
Improving Fine-Grained Control via Aggregation of Multiple Diffusion Models

Conghan Yue^{1,2} Zhengwei Peng¹ Shiyang Du¹ Zhi Ji^{3,2} Chuangjian Cai² Le Wan² Dongyu Zhang¹

Abstract

While many diffusion models perform well when controlling for particular aspect among style, character, and interaction, they struggle with fine-grained control due to dataset limitations and intricate model architecture design. This paper introduces a novel algorithm, Aggregation of Multiple Diffusion Models (AMDM), which synthesizes features from multiple diffusion models into a specified model, activating specific features for fine-grained control. Experimental results demonstrate that AMDM significantly improves fine-grained control without training, proving its effectiveness. Additionally, it reveals that diffusion models initially focus on features such as position, attributes, and style, with later stages improving generation quality and consistency. AMDM offers a new perspective for tackling the challenges of fine-grained conditional control generation in diffusion models: We can fully utilize existing or develop new conditional diffusion models that control specific aspects, and then aggregate them using AMDM algorithm. This eliminates the need for constructing complex datasets, designing intricate model architectures, and incurring high training costs. Code is available at: <https://github.com/Hammour-steak/AMDM>.

1. Introduction

Diffusion models (Sohl-Dickstein et al., 2015; Ho et al., 2020; Song et al., 2021a;b; Karras et al., 2022) have achieved excellent performance in generative tasks and the conditional diffusion models (Rombach et al., 2022; Chung et al., 2023; Esser et al., 2024) not only deliver advanced results in practical applications such as Text-to-Image (Nichol et al., 2022; Chen et al., 2023; Lee et al., 2024; Xu et al., 2024) and Image-to-Image generation (Zhang et al., 2023; Mou et al., 2024), but also offer highly flexible conditional

control mechanisms.

Recent research on conditional diffusion models has focused on achieving fine-grained control, including object attributes (Wu et al., 2023a; Wang et al., 2024a), interactions (Hoe et al., 2024; Jia et al., 2024), layouts (Zheng et al., 2023; Chai et al., 2023; Chen et al., 2024b), and style (Wang et al., 2023; Huang et al., 2024; Qi et al., 2024). However, maintaining consistency across diverse nuanced control remains a significant challenge. Generating multiple objects with overlapping bounding boxes can lead to attribute leakage, where the description of one object inappropriately influences others, causing inconsistencies between objects and the background. Fine-grained interaction details may be illogical, and style integration may compromise object attributes.

Existing approaches only partially address these issues due to the inherent complexity and diversity of fine-grained control, coupled with limitations in datasets and model architectures. Some works (Li et al., 2023; Zhou et al., 2024; Wang et al., 2024b) may perform well in preventing attribute leakage among multiple instances during layout generation but perform poorly in managing object interactions, while others (Ye et al., 2023; Huang et al., 2024) may excel in style transfer but exhibit limited control over layout.

Interestingly, most of these methods are based on Stable Diffusion (Rombach et al., 2022), which is theoretically grounded in DDPM (Ho et al., 2020) and classifier-free guidance (Dhariwal & Nichol, 2021) for conditional control. Therefore, for these conditional diffusion models grounded in the same theoretical foundation, our objective is to overcome this challenge by developing a method that effectively aggregates the advantages of each model, leveraging their unique strengths to achieve fine-grained control.

This paper proposes a novel algorithm called Aggregation of Multiple Diffusion Models (AMDM), as shown in Figure 1. AMDM aggregates intermediate variables from different conditional diffusion models which based on the same theoretical foundation, into a specific model during inference. This approach enhances features by absorbing characteristics from different models, regardless of variations in architecture or training datasets, without requiring additional training, avoiding the need for complex datasets and intricate model designs. Our experiments show that

¹Sun Yat-Sen University ²Game AI Center, Tencent University of Toronto. Correspondence to: Dongyu Zhang <zhangdy27@mail.sysu.edu.cn>.

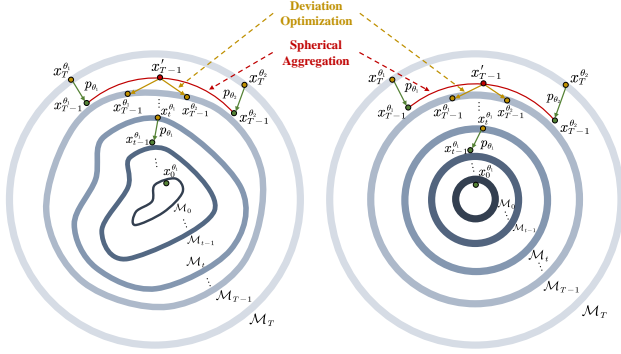


Figure 1: Geometry of AMDM in the data space (Left) and latent space (Right). The algorithm employs spherical aggregation and deviation optimization to incorporate conditional information during the initial steps. Subsequently, direct sampling is applied to expedite the process and generate high-quality images.

our proposed algorithm AMDM significantly improves the fine-grained generation capability of a specific conditional diffusion model. Furthermore, it demonstrates that diffusion models with a shared theoretical foundation allowing operations on their intermediate variables, while also revealing a phenomenon where early sampling steps focus on generating diverse features, and later stages prioritize quality and consistency.

Our main contributions are as follows:

- We propose a novel diffusion model aggregation algorithm, AMDM, that can aggregate intermediate variables from different conditional diffusion models of the same theoretical foundation, absorbing the characteristics of each model and enabling fine-grained generation.
- We conduct a variety of experiments, and both visual and quantitative results demonstrate noticeable improvements in areas where the models previously exhibited weaker control, validating the effectiveness of AMDM.
- AMDM reveals unique properties of diffusion models: intermediate variables from different diffusion models with a shared theoretical foundation can be manipulated. Additionally, diffusion models initially focus on generating features like position, attributes, and style, while later stages emphasize quality and consistency.

2. Preliminaries

2.1. Diffusion Models

Diffusion models are a class of generative models that progressively add noise to guide the data distribution $q(\mathbf{x}_0)$ towards a Gaussian distribution. In the classical DDPM (Ho

et al., 2020) formulation, the noise addition process from time $t - 1$ to t is defined as:

$$q(\mathbf{x}_t | \mathbf{x}_{t-1}) = \mathcal{N}(\sqrt{\alpha_t} \mathbf{x}_{t-1}, (1 - \alpha_t) \mathbf{I}), \quad (1)$$

where, \mathbf{x}_t represents the noisy data at timestep $t \in [0, T]$, α_t is the coefficient drift schedule generally satisfying $\lim_{t \rightarrow T} \alpha_t = 0$. From (1), we can readily derive the forward marginal distribution:

$$q(\mathbf{x}_t | \mathbf{x}_0) = \mathcal{N}(\sqrt{\bar{\alpha}_t} \mathbf{x}_0, (1 - \bar{\alpha}_t) \mathbf{I}), \quad (2)$$

where $\bar{\alpha}_t = \prod_{i=1}^t \alpha_i$. Equation (2) indicates that we can directly obtain \mathbf{x}_t from \mathbf{x}_0 avoiding multistep sampling. Assuming the generative model is $p_\theta(x_0)$, consider the variational lower bound of its likelihood as the loss function, i.e., the KL divergence of the joint probability:

$$\begin{aligned} \mathcal{L} &= KL(q(\mathbf{x}_{0:T}) || p_\theta(\mathbf{x}_{0:T})) \\ &\propto \mathbb{E}_{t, \mathbf{x}_t, \epsilon_t} [\|\epsilon_t - \epsilon_\theta(\mathbf{x}_t, t)\|^2], \end{aligned} \quad (3)$$

where $\epsilon_t \sim \mathcal{N}(\mathbf{0}, \mathbf{I})$ and $\epsilon_\theta(\mathbf{x}_t, t)$ is the denoising neural network. More generally, we utilize DDIM (Song et al., 2021a) sampling which directly defines the forward process (2) compared to DDPM. Ultimately, the reverse sampling process as follows:

$$\begin{aligned} p_\theta(\mathbf{x}_{t-1} | \mathbf{x}_t) &= \mathcal{N} \left(\sqrt{\frac{\bar{\alpha}_{t-1}}{\bar{\alpha}_t}} \mathbf{x}_t + \left(\sqrt{1 - \bar{\alpha}_{t-1} - \sigma_t^2} \right. \right. \\ &\quad \left. \left. - \sqrt{\frac{\bar{\alpha}_{t-1}(1 - \bar{\alpha}_t)}{\bar{\alpha}_t}} \right) \epsilon_\theta(\mathbf{x}_t, t), \sigma_t^2 \mathbf{I} \right), \end{aligned} \quad (4)$$

where σ_t is a free variable. When $\sigma_t^2 = \frac{1 - \bar{\alpha}_{t-1}}{1 - \bar{\alpha}_t} (1 - \frac{\bar{\alpha}_t}{\bar{\alpha}_{t-1}})$, it corresponds to DDPM sampling, while $\sigma_t^2 = 0$ results in a deterministic sampling, which is the origin of the name DDIM.

2.2. Classifier-Free Guidance

The key of conditional control in diffusion models is estimating $q(\mathbf{x}_{t-1} | \mathbf{x}_t, y)$ given the condition y . In unconditional generation, according to (4), it can be written as:

$$p_\theta(\mathbf{x}_{t-1} | \mathbf{x}_t) = \mathcal{N}(\boldsymbol{\mu}_\theta(\mathbf{x}_t, t), \sigma_t^2 \mathbf{I}). \quad (5)$$

Accordingly, Classifier-Free Guidance (Dhariwal & Nichol, 2021) directly incorporates the condition y into the mean for estimation:

$$\begin{aligned} p_\theta(\mathbf{x}_{t-1} | \mathbf{x}_t, y) &= \mathcal{N}(\boldsymbol{\mu}_\theta(\mathbf{x}_t, t, y), \sigma_t^2 \mathbf{I}) \\ &= \mathcal{N} \left(\sqrt{\frac{\bar{\alpha}_{t-1}}{\bar{\alpha}_t}} \mathbf{x}_t + \left(\sqrt{1 - \bar{\alpha}_{t-1} - \sigma_t^2} \right. \right. \\ &\quad \left. \left. - \sqrt{\frac{\bar{\alpha}_{t-1}(1 - \bar{\alpha}_t)}{\bar{\alpha}_t}} \right) \epsilon_\theta(\mathbf{x}_t, t, y), \sigma_t^2 \mathbf{I} \right). \end{aligned} \quad (6)$$

Therefore, the training loss function is:

$$\mathcal{L} \propto \mathbb{E}_{t, \mathbf{x}_t, \epsilon_t} [\|\epsilon_t - \epsilon_\theta(\mathbf{x}_t, t, y)\|^2]. \quad (7)$$

The noise model $\epsilon_\theta(\mathbf{x}_t, t, y)$ incorporates conditioning on y , guiding the denoising process towards the conditioned direction, thereby enabling conditional sampling and generation.

3. AMDM

In this section, we first analyze the challenges and limitations of current fine-grained control research, providing a general direction for potential solutions. Next, a rigorous formal definition of the research problem is presented for clarity, which makes it possible to aggregate intermediate variables for fine-grained control under certain conditions. Finally, we describe the design principles and propose the AMDM algorithm.

3.1. Analysis

Current fine-grained conditional control models tend to have limited control capabilities and face numerous issues. For example, given the caption "A red hair girl is drinking from a blue bottle of water, oil painting" and corresponding bounding boxes for positioning control, different models are likely to show varying performance, as illustrated in Figure 2. Model A, which receives additional inputs for position information and actions, excels in generating high-quality generation of positioning and interactions. However, it struggles with attribute control and maintaining the oil painting style. Conversely, Model B incorporates extra input for position and attribute information, managing both but not accurately capturing interactions and stylistic elements.

Caption: A red hair girl is drinking a blue bottle of water, oil painting

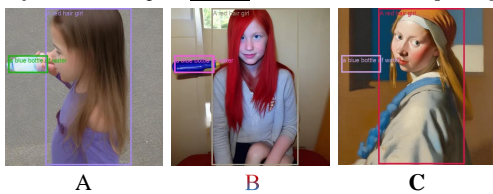


Figure 2: Examples of fine-grained conditional control of the same caption by different models.

Model C references the style of an image, enabling precise management of style characteristics but lacking adequate control over location and attribute details. The fundamental reason for these issues lies in the complexity and flexibility of fine-grained control tasks, which makes it challenging for limited datasets and specific model architectures to account for all the intricate features. Although implementing a specific feature for a particular task is relatively straightforward, integrating these features for fine-grained control remains a significant challenge.

While different models may have varying additional input

conditions, these conditions are often mutually compatible, leading to consistent objectives, which allows the models to generate similar images within their respective generation domains. Theoretically, model A has the capability to generate images that meet all the composite conditions of the caption for fine-grained control, although a single sampling might not fully activate this capability. It is noteworthy that these models share a common theoretical foundation, as they are all predicated on the same diffusion process and Classifier-Free Guidance (CFG) conditional control mechanism. Recognizing this shared basis, our objective is to develop an algorithm that leverages these commonalities to integrate the distinctive characteristics of multiple models into a specific model, achieving fine-grained conditional control in a more direct and efficient manner.

3.2. Definition

It is necessary to formally define the above concepts to facilitate a more rigorous exposition of the research problem and derive the design motivation for the aggregation algorithm.

Definition 3.1. For the diffusion model p_θ , its **generation domain** at t under condition y is:

$$D_{t,y}^\theta = \{\mathbf{x}_t \in \mathbb{R}^n \mid \mathbf{x}_t \sim p_\theta(\mathbf{x}_t|y)\}. \quad (8)$$

The generation domain $D_{t,y}^\theta$ represents the set of all intermediate variables at t generated by model θ under the condition y . Clearly, $D_{t,y}^\theta \subset \mathcal{M}_t$, where $\mathcal{M}_t = \{\mathbf{x}_t \in \mathbb{R}^n, \mathbf{x}_t \sim p(\mathbf{x}_t)\}$ which is independent of θ . Therefore, operations in different generation domains of t can be transformed on \mathcal{M}_t , which is independent of the model. This provides the possibility for the development of subsequent aggregation algorithms.

Definition 3.2. For a set of different diffusion models $M = \{p_{\theta_1}, p_{\theta_2}, \dots, p_{\theta_N}\}$, and corresponding conditions $Y = \{y_1, y_2, \dots, y_N\}$, if $\bigcap_{i=1}^N D_{t,y_i}^{\theta_i} \neq \emptyset$, then M is referred to as the **t -compatible model set** under condition Y .

This indicates that there exists an intersection on the manifold where \mathbf{x}_t resides under different conditions corresponding to various diffusion models within M . Evidently, the points at these intersections encapsulate all the information of the condition Y . Therefore, intermediate variables \mathbf{x}_t of any model encapsulate all conditional information, enabling the generation of images under additional composite conditions.

For a specific fine-grained control task, although different models may accept varying additional input types, they share a common objective. If this task is decomposed into different conditions y_1, y_2, \dots, y_N recognizable by different models, there must exist intermediate variables \mathbf{x}_t that

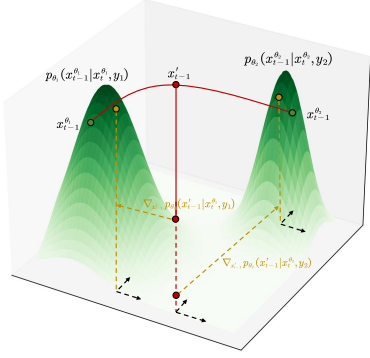


Figure 3: Geometry of deviation optimization between two models. The green points represent the original sampled points, the red points indicate the results of spherical aggregation, and the gold points denote the final results after deviation optimization.

satisfy each of these conditions for any $t \in [0, T]$. Consequently, these models collectively form a t -compatible model set under the condition $Y = \{y_1, y_2, \dots, y_n\}$. Given this, we have the following assumption:

Assumption 3.3. If y_1, y_2, \dots, y_n all describe a specific task, $M = \{p_{\theta_1}, p_{\theta_2}, \dots, p_{\theta_N}\}$ forms a t -compatible model set under the condition $Y = \{y_1, y_2, \dots, y_n\}$ for any $t \in [0, T]$.

In practical applications, we focus on generation for a specific task. Based on this assumption, these models form a t -compatible model set under the task condition Y , enabling generation under composite conditions and achieving fine-grained control.

3.3. Algorithm

For simplicity, we begin by considering the case of two models, specifically focusing on aggregating the conditional control information from p_{θ_2} into p_{θ_1} .

Manifold Consistency. In the previous section, we explored the theoretical foundation underlying the operations of different fine-grained control models. The key aspect is that the generation domain $D_{t,y}^{\theta}$ is a subdomain of \mathcal{M}_t which is independent of the model θ . Therefore, ensuring the consistency of \mathcal{M}_t guarantees the closure of intermediate variable operations across different $D_{t,y}^{\theta}$. Consequently, this requires the same diffusion process to ensure the consistency of the marginal distribution $p(\mathbf{x}_t)$ for each model, as well as aligned latent space encoders if they exist.

Spherical Aggregation. Sampling \mathbf{x}_0 from the model p_{θ_1} involves a series of reverse diffusion steps: $p_{\theta_1}(\mathbf{x}_T) \sim N(\mathbf{0}, \mathbf{I})$, $p_{\theta_1}(\mathbf{x}_{T-1}^{\theta_1} | \mathbf{x}_T^{\theta_1}, y_1)$, \dots , $p_{\theta_1}(\mathbf{x}_0^{\theta_1} | \mathbf{x}_1^{\theta_1}, y_1)$, signifying that $\mathbf{x}_t^{\theta_1} \in D_{t,y_1}^{\theta_1}$ for all $t \in [0, T]$. It indicates

that the new intermediate variable must also reside within $D_{t,y_i}^{\theta_1} \subset \mathcal{M}_t$ for the sampling of p_{θ_1} , after aggregating another model p_{θ_2} . To find the optimal aggregation strategy, we next consider the properties of \mathcal{M}_t .

In the data space, Chung et al. (2022) have proven that \mathcal{M}_t is concentrated on an $(n-1)$ -dimensional manifold, which approximates an n -dimensional hypersphere as t becomes large. In the latent space, \mathcal{M}_t will always be concentrated on the n -dimensional hypersphere for any t . The relevant proof can be found in Appendix B. This motivates the use of spherical linear interpolation as the aggregation strategy, which maximizes the retention of the aggregated data on the original manifold with minimal deviations:

$$\begin{aligned} \mathbf{x}'_{t-1} &= \text{Slerp}(\mathbf{x}_{t-1}^{\theta_1}, \mathbf{x}_{t-1}^{\theta_2}, w) \\ &= \frac{\sin((1-w)\theta)}{\sin(\theta)} \mathbf{x}_{t-1}^{\theta_1} + \frac{\sin(w\theta)}{\sin(\theta)} \mathbf{x}_{t-1}^{\theta_2}, \quad (9) \\ \theta &= \cos^{-1}(\mathbf{x}_{t-1}^{\theta_1} \cdot \mathbf{x}_{t-1}^{\theta_2}) \end{aligned}$$

where \mathbf{x}'_{t-1} represents the aggregated intermediate variable, $\mathbf{x}_{t-1}^{\theta_1}$ and $\mathbf{x}_{t-1}^{\theta_2}$ are sampled from $p_{\theta_1}(\mathbf{x}_{t-1}^{\theta_1} | \mathbf{x}_t^{\theta_1}, y_1)$ and $p_{\theta_2}(\mathbf{x}_{t-1}^{\theta_2} | \mathbf{x}_t^{\theta_2}, y_2)$ respectively, and $w \in [0, 1]$ is the weighting factor that balances the contribution of each model. Spherical aggregation integrates the conditional control information of p_{θ_2} into p_{θ_1} , while remaining the new variables stable near the manifold.

Deviation Optimization. Ideally, \mathbf{x}'_{t-1} would reside on $D_{t-1,y_1}^{\theta_1} \cap D_{t-1,y_2}^{\theta_2}$, but deviations are likely to occur in practice. Considering the step from t to $t-1$, since $p_{\theta_1}(\mathbf{x}_{t-1}^{\theta_1} | \mathbf{x}_t^{\theta_1}, y_1)$ follows a normal distribution, a single sample is to be drawn with high confidence, which suggests that $D_{t,y_1}^{\theta_1}$ is consistently concentrated near the mean. As a result, we can shift \mathbf{x}'_{t-1} along the gradient of the probability density function $p_{\theta_1}(\mathbf{x}_{t-1}^{\theta_1} | \mathbf{x}_t^{\theta_1}, y_1)$ by performing gradient ascent, adjusting the value to position it near the mean and bringing it back to $D_{t-1,y_1}^{\theta_1}$. In light of this, we propose the main proposition of the deviation optimization:

Proposition 3.4. For the diffusion model p_{θ_1} and any new intermediate variable \mathbf{x}'_{t-1} , let:

$$\mathbf{x}_{t-1}^{\theta_1} = \mathbf{x}'_{t-1} - \eta_{t-1}^{\theta_1} \frac{\mathbf{x}'_{t-1} - \mu_{\theta_1}(\mathbf{x}'_{t-1}, t, y_1)}{\|\mathbf{x}'_{t-1} - \mu_{\theta_1}(\mathbf{x}'_{t-1}, t, y_1)\|}, \quad (10)$$

then, $\mathbf{x}_{t-1}^{\theta_1}$ is corrected onto $D_{t-1,y_1}^{\theta_1}$. Here, $\mu_{\theta_1}(\mathbf{x}'_{t-1}, t, y_1)$ is defined by (6), $\eta_{t-1}^{\theta_1}$ is a small optimization step size.

Proof is provided in Appendix A, and the geometry of deviation optimization is illustrated in Figure 3. Proposition 3.4 demonstrates that the intermediate variable can be corrected in a straightforward way to reside on $D_{t-1,y_1}^{\theta_1}$, thereby improving sampling quality. Furthermore, since

the new variable contains information from p_{θ_2} and under Assumption 3.3, we can infer that it indeed resides on $D_{t-1, y_1}^{\theta_1} \cap D_{t-1, y_2}^{\theta_2}$, thus fulfilling the expectation of aggregation. We also introduce an adjustable aggregation step s , allowing flexible control over whether to incorporate information from other models.

Combining equations (9) and (10), the algorithm for aggregation of two diffusion models is presented, comprising two key components: spherical aggregation and deviation optimization. Spherical aggregation aggregates the conditional control information from different models and ensures that the new intermediate variables remain stable near the manifold, while deviation optimization ensures more precise retention on the corresponding data manifold, enhancing sample quality. The algorithm iteratively performs spherical aggregation and deviation optimization for each model during the first s steps, followed by direct sampling from p_{θ_1} . Note that each step of spherical aggregation also necessitates deviation optimization for p_{θ_2} to preserve the relevant conditional information within it, facilitating the subsequent aggregation step. This algorithm can be readily extended to multiple models, leading to the final Aggregation of Multi Diffusion Models (AMDM) algorithm, as shown in Algorithm 1. Moreover, since $\mu_{\theta_i}(\mathbf{x}_t^{\theta_i}, t, y_i)$ can

Algorithm 1 AMDM

Input: t -compatible model set $M = \{p_{\theta_1}, p_{\theta_2}, \dots, p_{\theta_N}\}$ under condition $Y = \{y_1, y_2, \dots, y_N\}$ with the same diffusion process, aggregation step s , weighting factor w_1, w_2, \dots, w_{N-1} and optimization step $\eta_t^{\theta_1}, \eta_t^{\theta_2}, \dots, \eta_t^{\theta_N}$
 $\mathbf{x}_T^{\theta_1}, \mathbf{x}_T^{\theta_2}, \dots, \mathbf{x}_T^{\theta_N} \sim N(\mathbf{0}, \mathbf{I})$
for t in $[T : 1]$ **do**
 $\mathbf{x}_{t-1}^{\theta_1} \sim p_{\theta_1}(\mathbf{x}_{t-1}^{\theta_1} | \mathbf{x}_t^{\theta_1}, y_1)$
if $t > T - s$ **then**
 $\mathbf{x}_{t-1}^{\theta_i} \sim p_{\theta_i}(\mathbf{x}_{t-1}^{\theta_i} | \mathbf{x}_t^{\theta_i}, y_i), i \in [2, N]$
 $\mathbf{x}'_{t-1} = \text{Slerp}(\mathbf{x}_{t-1}^{\theta_1}, \dots, \mathbf{x}_{t-1}^{\theta_N}, w_1, \dots, w_{N-1})$
 $\mathbf{x}_{t-1}^{\theta_i} = \mathbf{x}'_{t-1} - \eta_t^{\theta_i} \frac{\mathbf{x}'_{t-1} - \mu_{\theta}(\mathbf{x}_{t-1}^{\theta_i}, t, y_i)}{\|\mathbf{x}'_{t-1} - \mu_{\theta}(\mathbf{x}_{t-1}^{\theta_i}, t, y_i)\|}, i \in [1, N]$
end if
end for
Output: $x_0^{\theta_1}$

reuse $\epsilon_{\theta_i}(\mathbf{x}_t^{\theta_i}, t, y_i)$ from the previous sampling step, the deviation optimization only introduces a single mathematical operation with no additional computational overhead, avoiding extra inference time.

4. Experiments

In this section, we first aggregate the classic conditional diffusion models to evaluate the effectiveness of the algorithm, followed by a series of ablation experiments to demonstrate its optimality. All experiments were conducted using a



Figure 4: Visual results of aggregating MIGC into InteractDiffusion applying the AMDM algorithm.

single RTX 3090 GPU.

4.1. InteractDiffusion and MIGC

InteractDiffusion (Hoe et al., 2024) is a T2I model that combines a pretrained Stable Diffusion (SD) model with a locally controlled interaction mechanism, enabling fine-grained control over the generated images and demonstrating effective interactivity. Similarly, MIGC (Zhou et al., 2024) is a T2I model that employs a divide-and-conquer strategy, achieving excellent performance in both attribute representation and isolation of generated instances.

InteractDiffusion primarily focuses on controlling subject-object interactions. However, due to the lack of explicit constraints on object attributes within the model architecture and dataset design, it exhibits suboptimal performance in attribute control. To address this, we attempt to aggregate the intermediate variables of MIGC p_{θ_2} into InteractDiffusion p_{θ_1} by applying the AMDM algorithm, introducing attribute control information, and denoting this as InteractDiffusion(+MIGC). The total sampling steps T are set to 50, the aggregation step s is set to 20, the weighting factor w is set to 0.5 and the optimization steps $\eta_t^{\theta_1}$ and $\eta_t^{\theta_2}$ are both set to 0.3. We use InteractDiffusion v1.0, and MIGC is modified to use the DDIM sampling method to align with the same diffusion process. Experimental results are shown in Figure 4. It is evident that aggregating the MIGC model into InteractDiffusion using our proposed AMDM algorithm significantly enhances its learned representations, leading to a notable improvement in instance attribute control, and confirming the algorithm’s effectiveness.

Evaluation Metrics. We will introduce some comprehensive metrics used to evaluate the aggregated models.

COCO-MIG Benchmark (Zhou et al., 2024) assess the

enhancement in attribute metrics. The COCO-MIG Benchmark is based on the COCO-position layout, where each instance is assigned a color attribute, requiring the generated instances to satisfy both position and color constraints. The process includes sampling layouts from COCO and categorizing layouts into five levels (L2-L6) based on the number of instances. Then, colors are assigned to each instance, global prompts are constructed, and a test file containing 800 entries is generated. The COCO-MIG metrics primarily include Instance Success Rate and mIoU Score. The Instance Success Rate measures the probability of each instance being generated correctly, while mIoU Score calculates the average of the maximum IoU for all instances; if the color attribute is incorrect, the IoU value is set to 0. Since the MIG-Benchmark does not contain interactive prompt, we set the "action" input in the InteractDiffusion model to "and".

FGAHOI (Ma et al., 2023) can measure interaction controllability. We use the FGAHOI model based on the Swin-Tiny architecture, as an HOI detector to evaluate the model’s ability to control interactions. HOI Detection Scores are categorized into two types: Default and Known Object. The Default setting is more challenging, as it requires distinguishing between irrelevant images.

Fréchet Inception Distance (Heusel et al., 2017) measures the Fréchet distance in distribution of Inception feature between the real images and the generated images.

CLIP Score (Radford et al., 2021) evaluates the alignment between images and text by measuring how well an image corresponds to a given textual description using the CLIP model’s similarity score.

The quantitative results of InteractDiffusion(+MIGC) are shown in the first two rows of Table 1. It can be observed that all metrics have significantly improved in InteractDiffusion(+MIGC) after aggregating MIGC’s conditional information. The attribute control metrics, in particular, show a marked improvement and approach the performance of the original MIGC model, validating the effectiveness of the algorithm. Interestingly, as shown in the last two rows of Table 2, the aggregated InteractDiffusion(+MIGC) even surpasses the original InteractDiffusion model in terms of interaction performance, further validating the effectiveness of the algorithm.

Conversely, we also attempt to enhance the interaction control of MIGC and explore the performance of MIGC(+InteractDiffusion). The parameter design remains consistent with the previous one. As shown in the first two rows of Table 2, after aggregating the interaction information from InteractDiffusion into MIGC, there is a significant improvement in various metrics, especially in interaction capability. Additionally, as observed in the last two rows



Figure 5: Visual results of aggregating IP-Adapter into InteractDiffusion applying AMDM algorithm.

of Table 1, the MIGC(+InteractDiffusion) maintains the original performance of MIGC in attribute control, further validating the effectiveness of the algorithm.

4.2. InteractDiffusion and IP-Adapter

IP-Adapter (Ye et al., 2023) is a lightweight I2I model that employs a decoupled cross-attention mechanism to separately process text and image features, enabling multimodal image generation. Due to its superior performance in preserving the style of the reference image, we propose integrating the style information from IP-Adapter p_{θ_3} into InteractDiffusion p_{θ_1} , denoted as InteractDiffusion(+IP-Adapter). The total sampling steps T are set to 10, the aggregation step s is set to 5, the weighting factor w is set to 0.5, ip scale is set to 0.8 and the optimization steps $\eta_t^{\theta_1}$ and $\eta_t^{\theta_3}$ are both set to 0.3. We utilized IP-Adapter based on SD1.5 while keeping InteractDiffusion unchanged. The experimental results are shown in Figure 5. It can be observed that IP-Adapter enhances the style representations of InteractDiffusion, fully activating its style controllability, which further validates the effectiveness of the algorithm.

4.3. InteractDiffusion, MIGC and IP-Adapter

Furthermore, we attempt to aggregate the attribute features from MIGC p_{θ_2} and the style features from IP-Adapter p_{θ_3} into InteractDiffusion p_{θ_1} to evaluate the effectiveness of the AMDM algorithm. The pretrained models for the three architectures remain consistent with those mentioned above. The total sampling step T set to 10, an aggregation step s set to 5, and weight factors w_1 and w_2 set to 0.5 and 0.65. The optimization steps $\eta_t^{\theta_1}$, $\eta_t^{\theta_2}$, and $\eta_t^{\theta_3}$ are all simply set to 0.3, respectively. The experimental results are presented

Method	Instance Success Rate (%) \uparrow						mIoU Score (%) \uparrow						CLIP Score \uparrow	
	L_2	L_3	L_4	L_5	L_6	Avg	L_2	L_3	L_4	L_5	L_6	Avg	Global	Local
InteractDiffusion	37.50	35.62	35.31	30.62	34.16	34.06	32.98	31.63	30.82	28.29	30.40	30.40	31.09	27.56
InteractDiffusion(+MIGC)	62.29	54.33	56.31	53.87	52.89	54.78	54.30	46.37	48.44	47.65	46.64	47.74	32.81	28.96
MIGC	64.06	56.04	58.43	56.00	49.89	55.46	54.43	49.33	50.48	48.67	44.74	48.53	32.78	28.61
MIGC(+InteractDiffusion)	60.00	50.20	50.46	48.25	46.97	49.78	52.58	44.27	43.39	42.67	41.50	43.69	32.41	28.55

Table 1: Quantitative results on the COCO-MIG benchmark and CLIP Score across different models.

Method	Default \uparrow		Known Object \uparrow		FID \downarrow	CLIP Score \uparrow
	Full	Rare	Full	Rare		
MIGC	16.87	18.05	17.84	19.02	30.53	27.36
MIGC(+InteractDiffusion)	26.04	21.73	27.02	22.89	22.32	27.55
InteractDiffusion	29.53	23.02	30.99	24.93	18.69	26.91
InteractDiffusion(+MIGC)	31.40	24.52	32.76	26.32	18.35	27.18

Table 2: Quantitative results on the HOI Detection Score, FID and CLIP Score across different models.

in Figure 6.

These experiments provide robust evidence for the effectiveness of the AMDM algorithm. Furthermore, it can be inferred from the aggregation steps that the diffusion models initially focus on features such as position, attributes, and style, while later stages emphasize generation quality and consistency.

4.4. Ablation Studies

The AMDM algorithm consists of two key components: spherical aggregation and deviation optimization, with the aggregation degree controlled by the number of aggregation steps s . Therefore, in this section, we primarily conduct ablation studies on these aspects in the aggregation experiments of InteractDiffusion(+MIGC).

We attempt a comparison with linear aggregation, and the results are shown in the Figure 7. It can be observed that when the number of aggregation steps is small ($s < 5$), linear aggregation performs slightly better than spherical aggregation. However, as the number of aggregation steps increases, spherical aggregation significantly outperforms linear aggregation across various metrics. This is because, with more aggregation steps, the cumulative error due to the deviation in the data manifold becomes increasingly larger in linear aggregation, which negatively impacts the image quality. As shown in Figure 8, the characteristic of manifold deviation in linear aggregation is evident. In contrast, spherical aggregation consistently minimizes the deviation of the aggregated variables from the spherical manifold, preserving the quality of the final image as much as possible. The deviation optimization further enhances the image quality, demonstrating its effectiveness. Considering both performance and efficiency, spherical aggregation reaches optimum at 20 steps in this experiment.



Figure 6: Visual results of aggregating MIGC and IP-Adapter into InteractDiffusion applying the AMDM algorithm.

We also investigated the optimization step of deviation optimization, with experimental results shown in the Table 3. Obviously, when the optimization step is set to 0.3, the best performance is achieved across all metrics. Moreover, the results outperform those achieved with 50 aggregation steps without optimization.

5. Related Works

Fine-Grained Generation. In addition to text-driven models (Nichol et al., 2022; Ramesh et al., 2022; Rombach et al., 2022; Li et al., 2024b; Podell et al., 2024), an increasing number of studies are exploring more advanced and finer-grained conditional control techniques. One of the most classical approaches is personalization controlled generation, including style generation (Sohn et al., 2023; Liu et al., 2023; Hertz et al., 2024; Chen et al., 2024a),

Deviation Optimization Step	Instance Success Rate (%) \uparrow							mIoU Score (%) \uparrow						CLIP Score \uparrow	
	L_2	L_3	L_4	L_5	L_6	Avg	L_2	L_3	L_4	L_5	L_6	Avg	Global	Local	
0	61.56	52.08	53.75	51.62	51.87	53.18	54.76	45.09	46.36	45.48	45.79	46.62	31.09	27.56	
0.1	57.60	53.26	53.89	52.40	52.08	53.26	53.27	45.53	46.86	46.31	45.80	46.83	31.43	27.87	
0.2	59.62	54.27	54.06	51.25	52.29	53.40	52.71	46.32	47.17	44.68	45.74	46.59	31.92	28.45	
0.3	62.29	54.33	56.31	53.87	52.89	54.78	54.30	46.37	48.44	47.65	46.64	47.74	32.81	28.96	
0.4	61.34	53.62	55.32	52.22	52.50	53.96	53.46	46.21	46.82	45.26	46.23	46.78	32.23	28.55	
0.5	58.30	53.43	55.14	51.76	51.76	53.27	52.88	45.03	46.52	44.95	45.51	46.14	31.15	27.78	

Table 3: Ablation results of different deviation optimization step on COCO-MIG benchmark in InteractDiffusion(+MIGC).

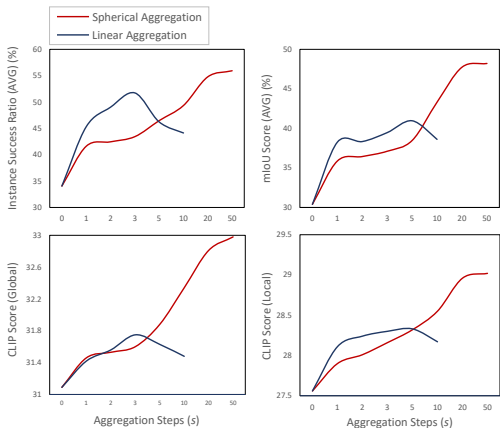


Figure 7: Metrics of spherical aggregation and linear aggregation under different aggregation steps.

subject-driven generation (Ruiz et al., 2023; Li et al., 2024a; Shi et al., 2024; Jiang et al., 2024; Ye et al., 2023), person-driven generation (Xiao et al., 2024; Giambi & Lisanti, 2023; Valevski et al., 2023; Achlioptas et al., 2023; Peng et al., 2024), and interactive generation (Huang et al., 2023b; Guo et al., 2024; Wu et al., 2023b; Hoe et al., 2024). Additionally, spatial-controlled generation (Li et al., 2023; Cheng et al., 2023; Kim et al., 2023; Nie et al., 2024; Zhou et al., 2024) represents another significant research focus, primarily leveraging bounding boxes or various regions as additional input conditions to achieve specific spatial control objectives. In recent years, several studies have attempted to directly achieve fine-grained control (Huang et al., 2023a; Han et al., 2023; Smith et al., 2023; Gu et al., 2024; Kumari et al., 2023) by designing various model architectures to handle inputs from various modalities, which require extensive training. These approaches inevitably necessitate a substantial amount of comprehensive multi-condition fine-grained data and the development of complex model architectures.

Compositional Generation. Some recent works (Hinton, 2002; Vedantam et al., 2018; Du et al., 2020; Liu et al., 2022; Du et al., 2023; Du & Kaelbling, 2024; Garipov et al., 2023) have attempted to combine multiple models with the aim of generating new distributions to enhance model generalization. Some of these studies (Du et al., 2020; 2023; Garipov

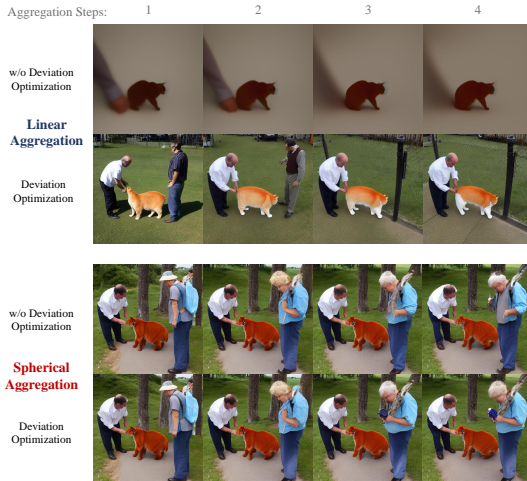


Figure 8: Visual results of deviation optimization for spherical aggregation and linear aggregation under different aggregation steps.

et al., 2023) focus on the combination of different objects, while others are primarily validated on toy examples (Hinton, 2002; Vedantam et al., 2018; Garipov et al., 2023), lacking practical relevance. In contrast, this paper focuses on fine-grained control for real-world tasks, strengthening consistency for the same object, and demonstrates significant improvements.

6. Conclusion

This paper proposes a novel AMDM algorithm, which consists of two main components: spherical aggregation and deviation optimization. Experimental results demonstrate the effectiveness of the AMDM algorithm, revealing that diffusion models initially prioritize image feature generation, shifting their focus to image quality and consistency in later stages. The algorithm provides a new perspective for addressing fine-grained generation challenge: We can leverage existing or develop new conditional diffusion models that control specific aspects, and then aggregate them using the AMDM algorithm. This eliminates the need for constructing complex datasets, designing intricate model architectures, and incurring high training costs.

References

- Achlioptas, P., Benetatos, A., Fostiropoulos, I., and Skourtis, D. Stellar: Systematic evaluation of human-centric personalized text-to-image methods. *arXiv preprint arXiv:2312.06116*, 2023.
- Chai, S., Zhuang, L., and Yan, F. Layoutdm: Transformer-based diffusion model for layout generation. In *Proceedings of the IEEE/CVF Conference on Computer Vision and Pattern Recognition*, pp. 18349–18358, 2023.
- Chen, D.-Y., Tennent, H., and Hsu, C.-W. Artadapter: Text-to-image style transfer using multi-level style encoder and explicit adaptation. In *Proceedings of the IEEE/CVF Conference on Computer Vision and Pattern Recognition*, pp. 8619–8628, 2024a.
- Chen, J., Huang, Y., Lv, T., Cui, L., Chen, Q., and Wei, F. Textdiffuser: Diffusion models as text painters. *Advances in Neural Information Processing Systems*, 36, 2024b.
- Chen, W., Hu, H., Saharia, C., and Cohen, W. W. Re-imaginer: Retrieval-augmented text-to-image generator. In *The Eleventh International Conference on Learning Representations*, 2023.
- Cheng, J., Liang, X., Shi, X., He, T., Xiao, T., and Li, M. Layoutdiffuse: Adapting foundational diffusion models for layout-to-image generation. *arXiv preprint arXiv:2302.08908*, 2023.
- Chung, H., Sim, B., Ryu, D., and Ye, J. C. Improving diffusion models for inverse problems using manifold constraints. In *Advances in Neural Information Processing Systems*, 2022.
- Chung, H., Kim, J., Mccann, M. T., Klasky, M. L., and Ye, J. C. Diffusion posterior sampling for general noisy inverse problems. In *The Eleventh International Conference on Learning Representations*, 2023.
- Dhariwal, P. and Nichol, A. Diffusion models beat gans on image synthesis. *Advances in neural information processing systems*, 34:8780–8794, 2021.
- Du, Y. and Kaelbling, L. P. Position: Compositional generative modeling: A single model is not all you need. In *Forty-first International Conference on Machine Learning*, 2024.
- Du, Y., Li, S., and Mordatch, I. Compositional visual generation with energy based models. *Advances in Neural Information Processing Systems*, 33:6637–6647, 2020.
- Du, Y., Durkan, C., Strudel, R., Tenenbaum, J. B., Dieleman, S., Fergus, R., Sohl-Dickstein, J., Doucet, A., and Grathwohl, W. S. Reduce, reuse, recycle: Compositional generation with energy-based diffusion models and mcmc. In *International conference on machine learning*, pp. 8489–8510. PMLR, 2023.
- Esser, P., Kulal, S., Blattmann, A., Entezari, R., Müller, J., Saini, H., Levi, Y., Lorenz, D., Sauer, A., Boesel, F., et al. Scaling rectified flow transformers for high-resolution image synthesis. In *Forty-first International Conference on Machine Learning*, 2024.
- Garipov, T., De Peuter, S., Yang, G., Garg, V., Kaski, S., and Jaakkola, T. Compositional sculpting of iterative generative processes. *Advances in neural information processing systems*, 36:12665–12702, 2023.
- Giambi, N. and Lisanti, G. Conditioning diffusion models via attributes and semantic masks for face generation. *arXiv preprint arXiv:2306.00914*, 2023.
- Gu, Y., Wang, X., Wu, J. Z., Shi, Y., Chen, Y., Fan, Z., Xiao, W., Zhao, R., Chang, S., Wu, W., et al. Mix-of-show: Decentralized low-rank adaptation for multi-concept customization of diffusion models. *Advances in Neural Information Processing Systems*, 36, 2024.
- Guo, Y., Yang, C., Rao, A., Liang, Z., Wang, Y., Qiao, Y., Agrawala, M., Lin, D., and Dai, B. Animatediff: Animate your personalized text-to-image diffusion models without specific tuning. In *The Twelfth International Conference on Learning Representations*, 2024.
- Han, L., Li, Y., Zhang, H., Milanfar, P., Metaxas, D., and Yang, F. Svdiff: Compact parameter space for diffusion fine-tuning. In *Proceedings of the IEEE/CVF International Conference on Computer Vision*, pp. 7323–7334, 2023.
- Hertz, A., Voynov, A., Fruchter, S., and Cohen-Or, D. Style aligned image generation via shared attention. In *Proceedings of the IEEE/CVF Conference on Computer Vision and Pattern Recognition*, pp. 4775–4785, 2024.
- Heusel, M., Ramsauer, H., Unterthiner, T., Nessler, B., and Hochreiter, S. Gans trained by a two time-scale update rule converge to a local nash equilibrium. *Advances in neural information processing systems*, 30, 2017.
- Hinton, G. E. Training products of experts by minimizing contrastive divergence. *Neural computation*, 14(8):1771–1800, 2002.
- Ho, J., Jain, A., and Abbeel, P. Denoising diffusion probabilistic models. *Advances in neural information processing systems*, 33:6840–6851, 2020.
- Hoe, J. T., Jiang, X., Chan, C. S., Tan, Y.-P., and Hu, W. Interactdiffusion: Interaction control in text-to-image diffusion models. In *Proceedings of the IEEE/CVF Conference on Computer Vision and Pattern Recognition*, pp. 6180–6189, 2024.

- Huang, L., Chen, D., Liu, Y., Shen, Y., Zhao, D., and Zhou, J. Composer: creative and controllable image synthesis with composable conditions. In *Proceedings of the 40th International Conference on Machine Learning*, pp. 13753–13773, 2023a.
- Huang, N., Zhang, Y., Tang, F., Ma, C., Huang, H., Dong, W., and Xu, C. Diffstyler: Controllable dual diffusion for text-driven image stylization. *IEEE Transactions on Neural Networks and Learning Systems*, 2024.
- Huang, Z., Wu, T., Jiang, Y., Chan, K. C., and Liu, Z. Reversion: Diffusion-based relation inversion from images. *arXiv preprint arXiv:2303.13495*, 2023b.
- Jia, X., Isobe, T., Li, X., Wang, Q., Mu, J., Zhou, D., Lu, H., Tian, L., Sirasao, A., Barsoum, E., et al. Customizing text-to-image generation with inverted interaction. In *ACM Multimedia 2024*, 2024.
- Jiang, Y., Wu, T., Yang, S., Si, C., Lin, D., Qiao, Y., Loy, C. C., and Liu, Z. Videobooth: Diffusion-based video generation with image prompts. In *Proceedings of the IEEE/CVF Conference on Computer Vision and Pattern Recognition*, pp. 6689–6700, 2024.
- Karras, T., Aittala, M., Aila, T., and Laine, S. Elucidating the design space of diffusion-based generative models. *Advances in Neural Information Processing Systems*, 35: 26565–26577, 2022.
- Kim, Y., Lee, J., Kim, J.-H., Ha, J.-W., and Zhu, J.-Y. Dense text-to-image generation with attention modulation. In *Proceedings of the IEEE/CVF International Conference on Computer Vision*, pp. 7701–7711, 2023.
- Kumari, N., Zhang, B., Zhang, R., Shechtman, E., and Zhu, J.-Y. Multi-concept customization of text-to-image diffusion. In *Proceedings of the IEEE/CVF Conference on Computer Vision and Pattern Recognition*, pp. 1931–1941, 2023.
- Lee, T., Yasunaga, M., Meng, C., Mai, Y., Park, J. S., Gupta, A., Zhang, Y., Narayanan, D., Teufel, H., Bellagente, M., et al. Holistic evaluation of text-to-image models. *Advances in Neural Information Processing Systems*, 36, 2024.
- Li, D., Li, J., and Hoi, S. Blip-diffusion: Pre-trained subject representation for controllable text-to-image generation and editing. *Advances in Neural Information Processing Systems*, 36, 2024a.
- Li, H., Shi, H., Zhang, W., Wu, W., Liao, Y., Wang, L., Lee, L.-h., and Zhou, P. Dreamscene: 3d gaussian-based text-to-3d scene generation via formation pattern sampling. *arXiv preprint arXiv:2404.03575*, 2024b.
- Li, Y., Liu, H., Wu, Q., Mu, F., Yang, J., Gao, J., Li, C., and Lee, Y. J. Gligen: Open-set grounded text-to-image generation. In *Proceedings of the IEEE/CVF Conference on Computer Vision and Pattern Recognition*, pp. 22511–22521, 2023.
- Liu, G., Xia, M., Zhang, Y., Chen, H., Xing, J., Wang, X., Yang, Y., and Shan, Y. Stylecrafter: Enhancing stylized text-to-video generation with style adapter. *arXiv preprint arXiv:2312.00330*, 2023.
- Liu, N., Li, S., Du, Y., Torralba, A., and Tenenbaum, J. B. Compositional visual generation with composable diffusion models. In *European Conference on Computer Vision*, pp. 423–439. Springer, 2022.
- Ma, S., Wang, Y., Wang, S., and Wei, Y. Fgahoi: Fine-grained anchors for human-object interaction detection. *IEEE Transactions on Pattern Analysis and Machine Intelligence*, 2023.
- Mou, C., Wang, X., Song, J., Shan, Y., and Zhang, J. Difieditor: Boosting accuracy and flexibility on diffusion-based image editing. In *Proceedings of the IEEE/CVF Conference on Computer Vision and Pattern Recognition*, pp. 8488–8497, 2024.
- Nichol, A. Q., Dhariwal, P., Ramesh, A., Shyam, P., Mishkin, P., Mcgrew, B., Sutskever, I., and Chen, M. Glide: Towards photorealistic image generation and editing with text-guided diffusion models. In *International Conference on Machine Learning*, pp. 16784–16804. PMLR, 2022.
- Nie, W., Liu, S., Mardani, M., Liu, C., Eckart, B., and Vahdat, A. Compositional text-to-image generation with dense blob representations. In *Forty-first International Conference on Machine Learning*, 2024.
- Peng, X., Zhu, J., Jiang, B., Tai, Y., Luo, D., Zhang, J., Lin, W., Jin, T., Wang, C., and Ji, R. Portraitbooth: A versatile portrait model for fast identity-preserved personalization. In *Proceedings of the IEEE/CVF Conference on Computer Vision and Pattern Recognition*, pp. 27080–27090, 2024.
- Podell, D., English, Z., Lacey, K., Blattmann, A., Dockhorn, T., Müller, J., Penna, J., and Rombach, R. Sdxl: Improving latent diffusion models for high-resolution image synthesis. In *The Twelfth International Conference on Learning Representations*, 2024.
- Qi, T., Fang, S., Wu, Y., Xie, H., Liu, J., Chen, L., He, Q., and Zhang, Y. Deadiff: An efficient stylization diffusion model with disentangled representations. In *Proceedings of the IEEE/CVF Conference on Computer Vision and Pattern Recognition*, pp. 8693–8702, 2024.

- Radford, A., Kim, J. W., Hallacy, C., Ramesh, A., Goh, G., Agarwal, S., Sastry, G., Askell, A., Mishkin, P., Clark, J., et al. Learning transferable visual models from natural language supervision. In *International conference on machine learning*, pp. 8748–8763. PMLR, 2021.
- Ramesh, A., Dhariwal, P., Nichol, A., Chu, C., and Chen, M. Hierarchical text-conditional image generation with clip latents. *arXiv preprint arXiv:2204.06125*, 1(2):3, 2022.
- Rombach, R., Blattmann, A., Lorenz, D., Esser, P., and Ommer, B. High-resolution image synthesis with latent diffusion models. In *Proceedings of the IEEE/CVF conference on computer vision and pattern recognition*, pp. 10684–10695, 2022.
- Ruiz, N., Li, Y., Jampani, V., Pritch, Y., Rubinstein, M., and Aberman, K. Dreambooth: Fine tuning text-to-image diffusion models for subject-driven generation. In *Proceedings of the IEEE/CVF conference on computer vision and pattern recognition*, pp. 22500–22510, 2023.
- Särkkä, S. and Solin, A. *Applied stochastic differential equations*, volume 10. Cambridge University Press, 2019.
- Shi, J., Xiong, W., Lin, Z., and Jung, H. J. Instantbooth: Personalized text-to-image generation without test-time finetuning. In *Proceedings of the IEEE/CVF Conference on Computer Vision and Pattern Recognition*, pp. 8543–8552, 2024.
- Smith, J. S., Hsu, Y.-C., Zhang, L., Hua, T., Kira, Z., Shen, Y., and Jin, H. Continual diffusion: Continual customization of text-to-image diffusion with c-lora. *arXiv preprint arXiv:2304.06027*, 2023.
- Sohl-Dickstein, J., Weiss, E., Maheswaranathan, N., and Ganguli, S. Deep unsupervised learning using nonequilibrium thermodynamics. In *International conference on machine learning*, pp. 2256–2265. PMLR, 2015.
- Sohn, K., Ruiz, N., Lee, K., Chin, D. C., Blok, I., Chang, H., Barber, J., Jiang, L., Entis, G., Li, Y., et al. Styledrop: text-to-image generation in any style. In *Proceedings of the 37th International Conference on Neural Information Processing Systems*, pp. 66860–66889, 2023.
- Song, J., Meng, C., and Ermon, S. Denoising diffusion implicit models. In *International Conference on Learning Representations*, 2021a.
- Song, Y., Sohl-Dickstein, J., Kingma, D. P., Kumar, A., Ermon, S., and Poole, B. Score-based generative modeling through stochastic differential equations. In *Proceedings of International Conference on Learning Representations (ICLR)*, 2021b.
- Valevski, D., Lumen, D., Matias, Y., and Leviathan, Y. Face0: Instantaneously conditioning a text-to-image model on a face. In *SIGGRAPH Asia 2023 Conference Papers*, pp. 1–10, 2023.
- Vedantam, R., Fischer, I., Huang, J., and Murphy, K. Generative models of visually grounded imagination. In *International Conference on Learning Representations*, 2018.
- Wang, R., Chen, Z., Chen, C., Ma, J., Lu, H., and Lin, X. Compositional text-to-image synthesis with attention map control of diffusion models. In *Proceedings of the AAAI Conference on Artificial Intelligence*, volume 38, pp. 5544–5552, 2024a.
- Wang, X., Darrell, T., Rambhatla, S. S., Girdhar, R., and Misra, I. Instancediffusion: Instance-level control for image generation. In *Proceedings of the IEEE/CVF Conference on Computer Vision and Pattern Recognition*, pp. 6232–6242, 2024b.
- Wang, Z., Zhao, L., and Xing, W. Stylediffusion: Controllable disentangled style transfer via diffusion models. In *Proceedings of the IEEE/CVF International Conference on Computer Vision*, pp. 7677–7689, 2023.
- Wu, Q., Liu, Y., Zhao, H., Kale, A., Bui, T., Yu, T., Lin, Z., Zhang, Y., and Chang, S. Uncovering the disentanglement capability in text-to-image diffusion models. In *Proceedings of the IEEE/CVF conference on computer vision and pattern recognition*, pp. 1900–1910, 2023a.
- Wu, R., Chen, L., Yang, T., Guo, C., Li, C., and Zhang, X. Lamp: Learn a motion pattern for few-shot-based video generation. *arXiv preprint arXiv:2310.10769*, 2023b.
- Xiao, G., Yin, T., Freeman, W. T., Durand, F., and Han, S. Fastcomposer: Tuning-free multi-subject image generation with localized attention. *International Journal of Computer Vision*, pp. 1–20, 2024.
- Xu, J., Liu, X., Wu, Y., Tong, Y., Li, Q., Ding, M., Tang, J., and Dong, Y. Imagereward: Learning and evaluating human preferences for text-to-image generation. *Advances in Neural Information Processing Systems*, 36, 2024.
- Ye, H., Zhang, J., Liu, S., Han, X., and Yang, W. Ip-adapter: Text compatible image prompt adapter for text-to-image diffusion models. *arXiv preprint arXiv:2308.06721*, 2023.
- Zhang, Y., Huang, N., Tang, F., Huang, H., Ma, C., Dong, W., and Xu, C. Inversion-based style transfer with diffusion models. In *Proceedings of the IEEE/CVF conference on computer vision and pattern recognition*, pp. 10146–10156, 2023.

Zheng, G., Zhou, X., Li, X., Qi, Z., Shan, Y., and Li, X. Layoutdiffusion: Controllable diffusion model for layout-to-image generation. In *Proceedings of the IEEE/CVF Conference on Computer Vision and Pattern Recognition*, pp. 22490–22499, 2023.

Zhou, D., Li, Y., Ma, F., Zhang, X., and Yang, Y. Migc: Multi-instance generation controller for text-to-image synthesis. In *Proceedings of the IEEE/CVF Conference on Computer Vision and Pattern Recognition*, pp. 6818–6828, 2024.

A. Proof of Proposition 3.4

Proposition 3.4. For the diffusion model p_{θ_1} and any new intermediate variable \mathbf{x}'_{t-1} , let:

$$\mathbf{x}_{t-1}^{\theta_1} = \mathbf{x}'_{t-1} - \eta_{t-1}^{\theta_1} \frac{\mathbf{x}'_{t-1} - \mu_{\theta_1}(\mathbf{x}_t^{\theta_1}, t, y_1)}{\|\mathbf{x}'_{t-1} - \mu_{\theta_1}(\mathbf{x}_t^{\theta_1}, t, y_1)\|}, \quad (10)$$

then, $\mathbf{x}_{t-1}^{\theta_1}$ is corrected onto $D_{t-1, y_1}^{\theta_1}$. Here, $\mu_{\theta_1}(\mathbf{x}_t^{\theta_1}, t, y_1)$ is defined by (6), $\eta_{t-1}^{\theta_1}$ is a small optimization step size.

Proof: Our objective is to correct the new variable \mathbf{x}'_{t-1} , which deviates from $D_{t-1, y_1}^{\theta_1}$, to ensure proper generation in subsequent sampling. Considering the step from t to $t-1$, since $p_{\theta_1}(\mathbf{x}_{t-1}^{\theta_1} | \mathbf{x}_t^{\theta_1}, y_1)$ follows a normal distribution, the sampling process typically results in high-confidence clustering near the mean, causing the data to consistently reside in this region. Thus, we can move \mathbf{x}'_{t-1} along the gradient of the probability density function $p_{\theta_1}(\mathbf{x}'_{t-1} | \mathbf{x}_t^{\theta_1}, y_1)$ by performing gradient ascent, thereby adjusting the value toward the peak region and aligning the data with the manifold $\mathcal{M} = \{\mathbf{x}_{t-1}^{\theta_1} \sim p_{\theta_1}(\mathbf{x}_{t-1}^{\theta_1} | \mathbf{x}_t^{\theta_1}, y_1)\}$. Since \mathcal{M} is a submanifold of $D_{t-1, y_1}^{\theta_1}$, this optimization approach effectively pulls \mathbf{x}'_{t-1} back onto $D_{t-1, y_1}^{\theta_1}$. Therefore, our optimization objective is:

$$\arg \max_{\mathbf{x}_{t-1}^{\theta_1} \in \bar{U}(\mathbf{x}'_{t-1}, \delta)} [\nabla_{\mathbf{x}'_{t-1}} p_{\theta_1}(\mathbf{x}'_{t-1} | \mathbf{x}_t^{\theta_1}, y_1)]^T (\mathbf{x}_{t-1}^{\theta_1} - \mathbf{x}'_{t-1}), \quad (11)$$

where $\bar{U}(\mathbf{x}'_{t-1}, \delta) = \{\mathbf{x} \mid \|\mathbf{x} - \mathbf{x}'_{t-1}\| \leq \delta\}$ and δ is a small adjusting step, then:

$$\begin{aligned} \mathbf{x}_{t-1}^{\theta_1} &= \mathbf{x}'_{t-1} + \delta \nabla_{\mathbf{x}'_{t-1}} p_{\theta_1}(\mathbf{x}'_{t-1} | \mathbf{x}_t^{\theta_1}, y_1) \\ &= \mathbf{x}'_{t-1} + \eta_{t-1}^{\theta_1} \frac{\nabla_{\mathbf{x}'_{t-1}} p_{\theta_1}(\mathbf{x}'_{t-1} | \mathbf{x}_t^{\theta_1}, y_1)}{\|\nabla_{\mathbf{x}'_{t-1}} p_{\theta_1}(\mathbf{x}'_{t-1} | \mathbf{x}_t^{\theta_1}, y_1)\|}, \end{aligned} \quad (12)$$

where $\eta_{t-1}^{\theta_1}$ is the step size for the unit gradient ascent. Since $p_{\theta_1}(\mathbf{x}'_{t-1} | \mathbf{x}_t^{\theta_1}, y_1)$ is a normal distribution, its gradient can be computed as follows:

$$\begin{aligned} \nabla_{\mathbf{x}'_{t-1}} p_{\theta_1}(\mathbf{x}'_{t-1} | \mathbf{x}_t^{\theta_1}, y_1) &= \frac{1}{(2\pi\sigma_t^2)^{n/2}} \nabla_{\mathbf{x}'_{t-1}} \left(e^{-\frac{\|\mathbf{x}'_{t-1} - \mu_{\theta_1}(\mathbf{x}_t^{\theta_1}, t, y_1)\|^2}{2\sigma_t^2}} \right) \\ &= -\frac{1}{(2\pi\sigma_t^2)^{n/2}} e^{-\frac{\|\mathbf{x}'_{t-1} - \mu_{\theta_1}(\mathbf{x}_t^{\theta_1}, t, y_1)\|^2}{2\sigma_t^2}} \left(\frac{\mathbf{x}'_{t-1} - \mu_{\theta_1}(\mathbf{x}_t^{\theta_1}, t, y_1)}{\sigma_t^2} \right). \end{aligned} \quad (13)$$

Simplifying the coefficient term, the final result is:

$$\mathbf{x}_{t-1}^{\theta_1} = \mathbf{x}'_{t-1} - \eta_{t-1}^{\theta_1} \frac{\mathbf{x}'_{t-1} - \mu_{\theta_1}(\mathbf{x}_t^{\theta_1}, t, y_1)}{\|\mathbf{x}'_{t-1} - \mu_{\theta_1}(\mathbf{x}_t^{\theta_1}, t, y_1)\|}, \quad (14)$$

which concludes the proof.

B. Concentration of Latent Diffusion

In this section, we investigate the concentration of the marginal distribution for Stable Diffusion.

Lemma B.1. (Concentration of Measure Theorem for High-Dimensional Independent Normal Distribution). Let $X = (X_1, X_2, \dots, X_n)$ be an n -dimensional random vector where each component X_i is independently and identically distributed as $\mathcal{N}(\mathbf{0}, \sigma^2 \mathbf{I})$. Then, as the dimension n increases, the norm $\|X\|$ of X is concentrated around $\sqrt{n}\sigma$. Specifically, for any small $\epsilon \geq 0$ and sufficiently large n ,

$$P\left(\left|\|X\| - \sqrt{n}\sigma\right| \leq \epsilon\sqrt{n}\sigma\right) \geq 1 - 2e^{-\frac{n\epsilon^2}{1+2\epsilon}} \quad (15)$$

This means X will concentrate near the hypersphere of radius $\sqrt{n}\sigma$ with high probability.

Proof: First, we consider the squared norm of a random vector $X : \|X\|^2 = X_1^2 + X_2^2 + \dots + X_n^2$. Since $X_i \sim \mathcal{N}(0, \sigma^2 \mathbf{I})$, it follows that $Y = \|X\|^2 / \sigma^2 \sim \chi^2(n)$.

Using the Chernoff bound of the chi-square distribution:

$$P(Y \geq (1 + \delta)n) \leq e^{-\frac{n}{2}[\delta - \ln(1 + \delta)]}, \quad (16)$$

$$P(Y \leq (1 - \delta)n) \leq e^{-\frac{n}{2}[-\delta - \ln(1 - \delta)]}, \quad (17)$$

where $\delta \geq 0$ is a small value. According to $\ln(1 + \delta) \leq \frac{(2 + \delta)\delta}{2(1 + \delta)}$ and $\ln(1 - \delta) \leq -\delta - \frac{\delta^2}{2}$, we can deduce that:

$$\begin{aligned} P(\|X\|^2 \geq (1 + \delta)n\sigma^2) &= P(Y \geq (1 + \delta)n) \\ &\leq e^{-\frac{n\delta^2}{4(1 + \delta)}} \end{aligned} \quad (18)$$

$$\begin{aligned} P(\|X\|^2 \leq (1 - \delta)n\sigma^2) &= P(Y \leq (1 - \delta)n) \\ &\leq e^{-\frac{n\delta^2}{4}} \\ &\leq e^{-\frac{n\delta^2}{4(1 + \delta)}} \end{aligned} \quad (19)$$

Given the $\sqrt{1 + \delta} \leq 1 + \frac{\delta}{2}$ and $\sqrt{1 - \delta} \geq 1 - \frac{\delta}{2}$, we have:

$$\begin{aligned} P(\|X\| \geq (1 + \frac{\delta}{2})\sqrt{n}\sigma) &\leq P(\|X\| \geq \sqrt{(1 + \delta)}\sqrt{n}\sigma) \\ &\leq e^{-\frac{n\delta^2}{4(1 + \delta)}} \end{aligned} \quad (20)$$

$$\begin{aligned} P(\|X\| \leq (1 - \frac{\delta}{2})\sqrt{n}\sigma) &\leq P(\|X\| \leq \sqrt{(1 - \delta)}\sqrt{n}\sigma) \\ &\leq e^{-\frac{n\delta^2}{4(1 + \delta)}} \end{aligned} \quad (21)$$

Let $\epsilon = \delta/2$, and then organize equations (20) and (21):

$$P(|\|X\| - \sqrt{n}\sigma| \leq \epsilon\sqrt{n}\sigma) \geq 1 - 2e^{-\frac{n\epsilon^2}{1 + 2\epsilon}} \quad (22)$$

which concludes the proof.

The continuous form of (1) can be rewrite as:

$$d\mathbf{x}_t = -\frac{1}{2}g_t^2 \mathbf{x}_t dt + g_t d\mathbf{w}_t, \quad (23)$$

where $g_t^2 = -\frac{1}{\alpha_t} \frac{d\alpha_t}{dt}$. We can use equations (5.50) and (5.51) (Särkkä & Solin, 2019) to derive the relationship between the mean and variance of (23) as they evolve over time:

$$\frac{d\mathbf{m}}{dt} = \mathbb{E} \left[-\frac{1}{2}g_t^2 \mathbf{x}_t \right] = -\frac{1}{2}g_t^2 \mathbf{m} \quad (24)$$

$$\begin{aligned} \frac{d\mathbf{P}}{dt} &= \mathbb{E} \left[-\frac{1}{2}g_t^2 \mathbf{x}_t (\mathbf{x}_t - \mathbf{m})^T \right] + \mathbb{E} \left[-\frac{1}{2}g_t^2 (\mathbf{x}_t - \mathbf{m}) \mathbf{x}_t^T \right] + g_t^2 \mathbf{I} \\ &= -g_t^2 \mathbf{P} + g_t^2 \mathbf{I} \end{aligned} \quad (25)$$

The solutions are:

$$\mathbf{m}(t) = \mathbf{m}(0) e^{-\frac{1}{2} \int_0^t g_s^2 ds} \quad (26)$$

$$\mathbf{P}(t) = \mathbf{I} + (\mathbf{P}(0) - \mathbf{I}) e^{-\int_0^t g_s^2 ds} \quad (27)$$

Since the initial distribution in the latent space is a standard Gaussian distribution, we set $\mathbf{m}(0) = \mathbf{0}$ and $\mathbf{P}(0) = \mathbf{I}$, resulting in:

$$\mathbf{m}(t) = \mathbf{0} \quad (28)$$

$$\mathbf{P}(t) = \mathbf{I} \quad (29)$$

This means that at any given time, the marginal distribution of Stable Diffusion is a standard Gaussian distribution. Combined with Lemma B.1, it follows that \mathcal{M}_t is concentrated on the n -dimensional hypersphere.

C. Additional Visual Results



Figure 9: Additional Visual results of aggregating MIGC into InteractDiffusion applying the AMDM algorithm.



Figure 10: Additional Visual results of aggregating IP-Adapter into InteractDiffusion applying AMDM algorithm.

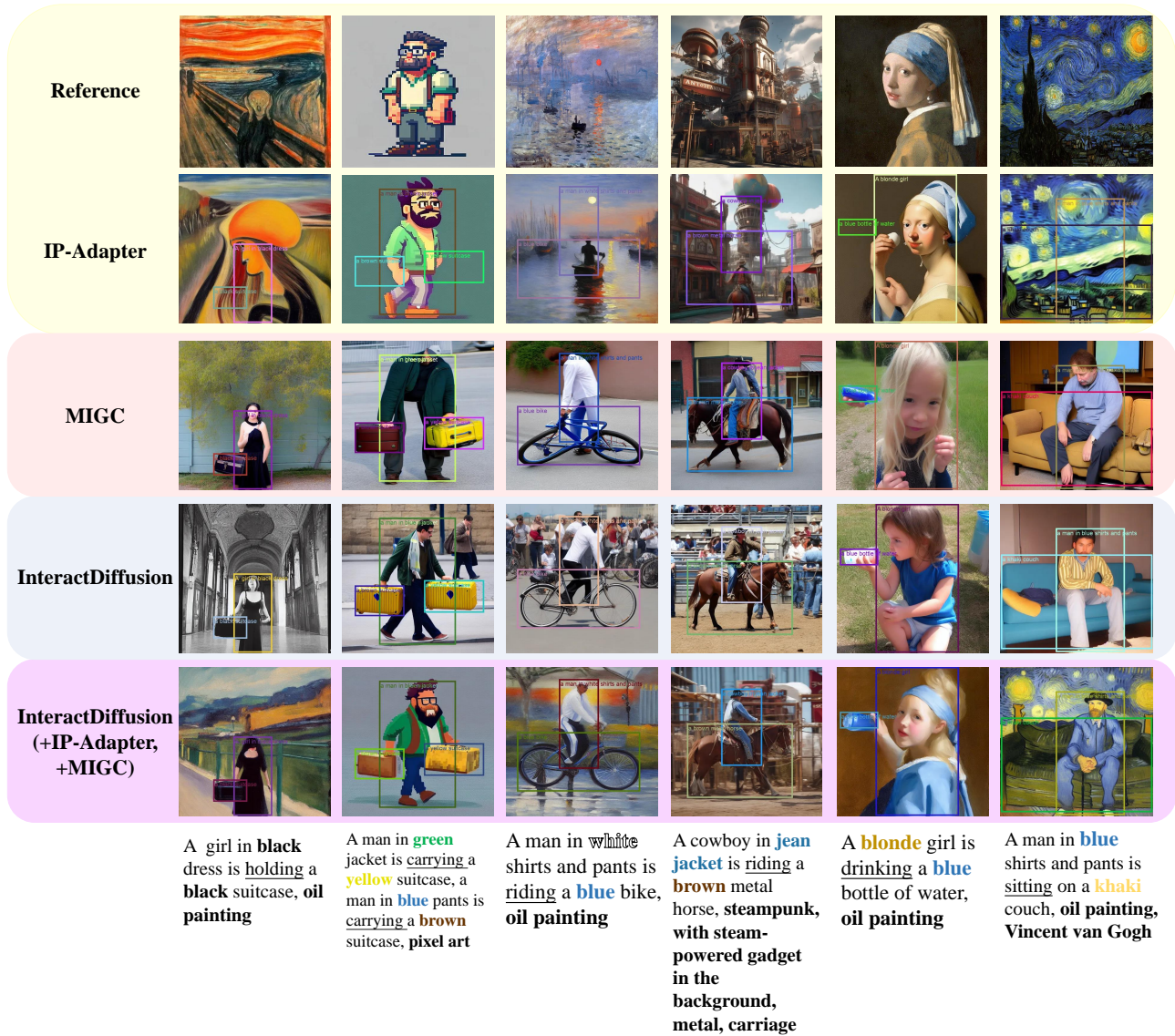


Figure 11: Additional Visual results of aggregating MIGC and IP-Adapter into InteractDiffusion applying the AMDM algorithm.